Progress in Oceanography 229 (2024) 103363

Contents lists available at ScienceDirect

Progress in Oceanography

journal homepage: www.elsevier.com/locate/pocean

Stable carbon isotopic composition of particulate organic matter in the Cosmonaut and Cooperation Seas in summer

Jiawen Kang [a], Qiang Hao [b], Shunan Cao [c], Jun Zhao [b], Zifei Yang [a], Zhen Tang [a], Minfang Zheng [a], Yusheng Qiu [a], Mengya Chen [a], Jianming Pan [b], Jianfeng He [c], Min Chen [a,*]

[a] College of Ocean and Earth Sciences, Xiamen University, Xiamen 361102, China
[b] Second Institute of Oceanography, Ministry of Natural Resources, Hangzhou 310012, China
[c] Polar Research Institute of China, Ministry of Natural Resources, Shanghai 201209, China

ARTICLE INFO

Keywords:
Particulate organic carbon
Carbon isotopes
Phytoplankton composition
Cosmonaut Sea
Cooperation Sea

ABSTRACT

This study examined particulate organic carbon (POC) and its isotopic composition ($\delta^{13}C_{POC}$) in the Cosmonaut and Cooperation Seas in the Antarctica during the summer of 2019. Our results show that the spatial variation of POC concentration in summer surface water generally mirrors that of $\delta^{13}C_{POC}$, with higher POC and $\delta^{13}C_{POC}$ values in the Cosmonaut Sea compared to the Cooperation Sea. The $\delta^{13}C_{POC}$ values in both seas were positively correlated with the proportion of Chl-a in smaller particles (< 20 μm). However, the relationship with the proportion of biogenic POC in smaller particles (< 20 μm) differed between the two seas. This discrepancy is attributed to differences in the dominant phytoplankton species. In the Cosmonaut Sea, smaller phytoplankton (nano- and pico-phytoplankton) were dominated by *Phaeocystis antarctica*, whereas in the Cooperation Sea, they were dominated by pennate diatoms. The $\delta^{13}C_{POC}$ in deep waters of both seas increased with depth, reflecting the effects of organic remineralization. The carbon isotope fractionation factors during remineralization, estimated using Rayleigh model, were 1.5 ± 0.2‰ and 1.6 ± 0.2‰ in the Cosmonaut Sea and the Cooperation Sea, respectively. These small isotope effects indicate that the isotope signals of organic matter exported from the upper layer are well preserved in the deep ocean. Additionally, anomalously high $\delta^{13}C_{POC}$ values were observed in the bottom water outside the Cape Darnley polynya in the Cooperation Sea, reflecting the input of ice algae-derived organic matter from the shelf during AABW formation. A simple isotopic mass balance estimate suggests that 6–19% of the POC in the AABW of the Cooperation Sea is contributed by ice algae. Our study highlights the complexity of factors affecting $\delta^{13}C_{POC}$ in the Southern Ocean, emphasizing the importance of phytoplankton community composition.

1. Introduction

The Southern Ocean is a crucial region for the global carbon cycle and climate change (Sarmiento and LeQuéré, 1996). The eastward Antarctic Circumpolar Current (ACC), driven by strong westerly winds, connects the Atlantic, Indian, and Pacific Oceans, serving as the primary conduit for the transport of heat, salinity, and organic matter (Pollard et al., 2002, Talley et al., 2016). The euphotic zone in the Southern Ocean, characterized by high nutrients and low chlorophyll a (Chl-a), has sparked ongoing interest in the environmental factors that regulate primary productivity (Tripathy et al., 2015). Light availability and iron supply are two critical factors influencing primary productivity in the Southern Ocean (Nelson and Smith,1991; Smith and Lancelot, 2004; Arrigo et al., 2015). Numerous studies have shown that the upwelling regions and the marginal ice zone (MIZ) exhibit higher primary productivity due to increased light and Fe availability (Moore and Abbott, 2000; Smith and Nelson, 1985). Iron released from melting sea ice and enhanced stratification are key factors that boost primary productivity in the MIZ (Moline and Prézelin, 1996; Garibotti et al., 2003; Lannuzel et al., 2008). Primary productivity is the main source of particulate organic carbon (POC) and thus drives the biological pump in the Southern Ocean (Benner and Amon, 2015). Therefore, a comprehensive understanding of the production, degradation, and burial of POC in the Southern Ocean is vital for better understanding of the global carbon cycle and climate change.

The subpolar zone of the Southern Ocean, located between the

* Corresponding author.
E-mail address: mchen@xmu.edu.cn (M. Chen).

https://doi.org/10.1016/j.pocean.2024.103363
Received 12 July 2024; Received in revised form 13 September 2024; Accepted 6 October 2024
Available online 15 October 2024
0079-6611/© 2024 Elsevier Ltd. All rights are reserved, including those for text and data mining, AI training, and similar technologies.

southern boundary (SB) of the ACC and the Antarctic Slope Front (ASF), not only exhibits large-scale meridional and zonal circulation (Wakatsuchi et al., 1994; Whitworth et al., 1985; Bindoff et al., 2000), but also significant sea ice formation and retreat (Gloersen et al., 1992). These environmental conditions promote the growth of phytoplankton, providing abundant food for zooplankton, fish and mammals. Garrity et al. (2005) demonstrated that regions with annual sea ice coverage concentrations ranging from 9% to 67% have higher carbon export fluxes, indicating that subpolar zones are crucial to the Southern Ocean carbon cycle. Particulate organic carbon in the subpolar Southern Ocean is primarily derived from primary production and biogenic detritus of ice algae and phytoplankton (Fabiano et al., 1996; Pasquer et al., 2010; Arrigo et al., 2012; Misic et al., 2017; Venturini et al., 2020). The carbon isotopic composition of organic matter ($\delta^{13}C_{POC}$) derived from ice algae and phytoplankton varies, reflecting different biogeochemical processes and isotope fractionation effects. This variation is used to determine the source and transformation of POC. $\delta^{13}C_{POC}$ has been employed to identify the source of organic matter (Gibson et al., 1999; Jia et al., 2020; Venturini et al., 2020) and to provide various biogeochemical insights, such as the growth, species and size of phytoplankton (Bentaleb et al., 1998; Lara et al., 2010; Henley et al., 2012; Stirnmann et al., 2024), pathways and mechanisms in photosynthetic carbon fixation (Bentaleb et al.,1998; Wilkes and Pearson, 2019), and remineralization of POC in deep water (Venturini et al., 2020; Close and Henderson, 2020). However, isotope studies on POC in the Southern Ocean have predominantly focused north of the Polar Front (Dehairs et al., 1997; Cavagna et al., 2013; Soares et al., 2020), with only a few reports from the Weddell Sea (Kennedy et al., 2002), Antarctic Peninsula (Henley et al., 2012), Prydz Bay (Ren et al., 2015), and circum-Antarctic surface waters in the subpolar zones. To address this gap, our study investigates the carbon isotopic composition of particulate organic matter in the subpolar region of the Indian Ocean sector of the Southern Ocean.

Knowledge of the carbon cycle in the Indian Ocean sector of the Southern Ocean remains limited. In the summer of 2006, researchers conducted a comprehensive multidisciplinary survey of the eastern Weddell-Enderby Basin (30 – 80 °E) (Nicol et al., 2010; Westwood et al., 2010; Davidson et al., 2010; Williams et al., 2010; Pasquer et al., 2010). Studies have indicated that primary productivity in the MIZ is significantly higher than in the open ocean, with an average of 2110 ± 1347 mgC/m^2/d (Westwood et al., 2010). The spatial variation of POC concentration is influenced by the retreat of sea ice and ocean currents (Pasquer et al., 2010). In this study, we measured the carbon isotopic composition of particulate organic matter in the Cosmonaut Sea (30 – 55 °E) and the Cooperation Sea (55 – 80 °E) within the Weddell-Enderby Basin. Our aim is to identify the main biological factors causing the spatial variation of $\delta^{13}C_{POC}$ and to explore the potential of using $\delta^{13}C_{POC}$ to trace the formation of AABW in the Cooperation Sea.

2. Materials and methods

2.1. Study area

The study area is situated in the Weddell-Enderby Basin, ranging from 30 °E to 80 °E in the Indian Ocean sector of the Southern Ocean. It encompasses the Cosmonaut Sea (30–55 °E) and the Cooperation Sea (55 – 80 °E) (Fig. 1). The region features an eastward-flowing ACC between 60 °S and 62 °S in the north, and a westward-flowing Antarctic Slope Current (ASC) in the south. The ASC is a robust current along the continental slope at depths of 750–1250 m (Williams et al., 2010). The area between the ASC and the southern boundary (SB) of the ACC is referred to as the subpolar zone, the primary region influenced by ACC upwelling through Ekman transport (Williams et al., 2010). Some studies also identify the fixed latitude of 64 °S as the core upwelling area (Pakhomov, 2000). In the eastern Cooperation Sea, a southward-flowing

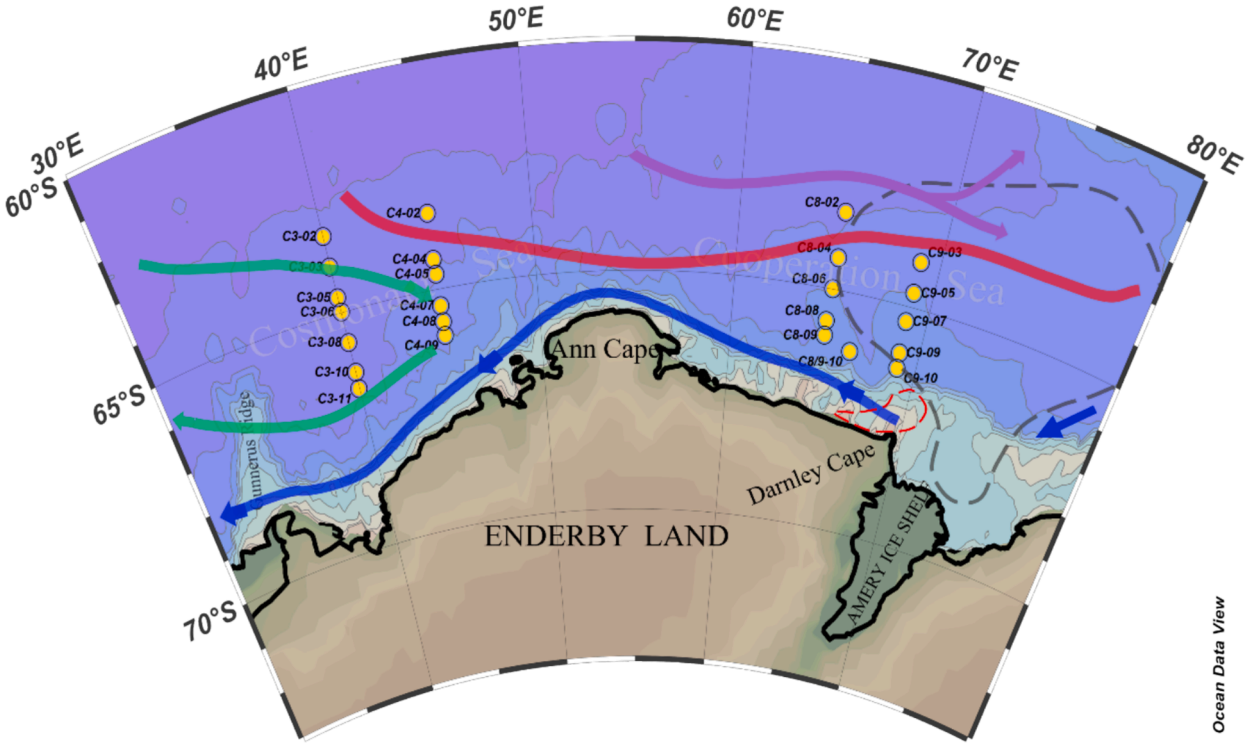

Figure 1. Sampling locations in the Cosmonaut Sea and the Cooperation Sea. The boundary between the Cosmonaut Sea and the Cooperation Sea is approximately 55°E, with the Cosmonaut Sea to the west and the Cooperation Sea to the east. The sampling sites are indicated by yellow circles. Major currents and fronts are marked with different colored lines: the purple, red, blue, and green lines represent the southerly ACC front (sACC), the Southern Boundary of ACC (SB), the Antarctic slope current, and the eastern boundary of the Weddell Gyre, respectively (Orsi et al., 1995). The grey dotted line represents the Prydz Gyre (Heywood et al., 1999). The red dashed frame depicts the Cape Darnley polynya (Ohshima et al., 2013).

ACC, driven by topography, and a westward-flowing ASC form the clockwise Prydz Bay Gyre (Smith et al., 1984; Heywood et al., 1999). The western Cosmonaut Sea is affected by the eastern thumb of the Weddell Gyre, resulting in a small clockwise subsurface recirculation at 37 °E influenced by the Gunnerus Ridge. This recirculation brings warm, deep water to the surface, creating a perennial polynya (Comiso and Gordon 1996; Geddes and Moore, 2007).

The water masses influencing our study area include summer surface water (SSW), winter residual water (WW), thermocline water (TCW), circumpolar deep water (CDW), dense shelf water (DSW), and Antarctic bottom water (AABW). Under the influence of solar radiation and ice melting, SSW has a temperature above -0.5 °C and a salinity between 33.0 and 34.5. WW occupies the subsurface and forms the minimum temperature layer (T_{min}), characterized by low temperature and high salinity (T < -1 °C, S = 34.2 - 34.5). In regions of the continental shelf and sea-ice margins, SSW often does not exist but instead exhibits the characteristics of WW (Williams et al., 2010). The large density difference between SSW and WW cause strong stratification of the water column, forming a seasonal surface mixed layer (SML). The permanent thermocline water (TCW, -1.0 °C < T < 0.5 °C, 34.4 < S < 34.5) lies between T_{min} and the CDW (0.5 °C < T < 2 °C, S > 34.4), separating the upper waters from the deeper waters. The CDW rises along the continental slope to a depth of about 150 m and mixes with the DSW to form a modified CDW with a temperature of 0−1.5 °C and a salinity higher than 34.4 (Orsi et al., 1995, 1999; Williams et al., 2010; Talley et al., 2011). The formation of AABW has been observed at Darnley Cape, northwest of Prydz Bay, indicating that our study area is one of the sources of AABW (Meijers et al., 2010; Ohshima et al., 2013; Jia et al., 2022).

The melting of sea ice in the study area exhibits spatiotemporal variability. In late spring and early summer (from November to January of the following year), the sea ice gradually melts from northeast to southwest, indicating that sea ice in the Cooperation Sea melts earlier than in the Cosmonaut Sea. In fact, small amounts of ice floes often persist in the Cosmonaut Sea in January (Raymond et al., 2009; Williams et al., 2010). The SML becomes shallower under the influence of melting sea ice, averaging around 25 m in the Cosmonaut Sea and about 50 m in the Cooperation Sea. Variations in SML depth affect light availability, potentially altering phytoplankton community structure. Previous studies have shown that the growth of *Phaeocystis* spp. in the Cosmonaut Sea is associated with a shallower mixed layer (Davidson et al., 2010; Wright et al., 2010). Additionally, algal biomass, particularly ice algae, is generally higher at the bottom of sea ice, with thicker ice supporting greater biomass. The melting sea ice promotes algal blooms in the surrounding waters, providing a food source for zooplankton and benthos in the open ocean (Grose and McMinn, 2003; McMinn et al., 2007; Van Leeuwe et al., 2018).

2.2. Sampling

Seawater samples were collected from 24 stations across four meridional sections in the Cosmonaut and Cooperation Seas (30-80 °E, 60-67 °S) aboard the R/V *Xuelong 2* in December 2019 (Fig. 1). At sections C8 and C9, samples were taken from the entire water column, whereas at the other stations, samples were collected only from depths shallower than 200 m. The seawater samples were collected using CTD rosettes and immediately filtered through pre-combusted (450 °C, 4 h) Whatman GF/F filters. The samples were then dried at 60 °C, stored at -20 °C, and transported back to the onshore laboratory.

2.3. Measurement of POC, PN and $\delta^{13}C_{POC}$

In the onshore laboratory, a subsample of the filter was fumigated with concentrated hydrochloric acid to remove inorganic carbon. The sample, now free of inorganic carbon and fully dried, was wrapped in a tin capsule and analyzed using a mass spectrometer (Thermo Finnigan Delta V) interfaced with an elemental analyzer (Thermo Flash EA 1112) to measure POC and its isotopes. For particulate nitrogen (PN) determination, a subsample was directly wrapped in a tin capsule and analyzed using the same instrument. The content of POC and PN in the sample was calculated using a calibration curve established with the $C_6H_6N_2O$ standard (Elemental Microanalysis Limited). The detection limits for POC and PN were 0.1 μmol C and 0.1 μmol N, respectively, with measurement accuracies better than 0.2%. To ensure the accuracy of isotopic data, one IAEA-C8 standard ($\delta^{13}C$ = -18.3‰, International Atomic Energy Agency) and one USGS40 standard ($\delta^{13}C$ = -26.4‰, United States Geological Survey) were inserted into every 10 samples for simultaneous measurement. A working curve was established using these two standards to create a two-point calibration, and the $\delta^{13}C$ values of the samples were calculated accordingly. The $\delta^{13}C_{POC}$ values relative to the Peedee Belemnite (PDB) standard were defined as follows:

$$\delta^{13}C_{POC} = \left(\frac{R_{sample}}{R_{Standard}} - 1\right) \times 1000‰ \quad (1)$$

where R_{sample} represents the $^{13}C/^{12}C$ ratio in the sample measured by the mass spectrometer, and $R_{standard}$ represents the $^{13}C/^{12}C$ ratio in PDB. Our multiple measurement results indicate that the average $\delta^{13}C$ values for USGS40 and IAEA-C8 are -25.44 ± 0.09‰ and -17.43 ± 0.17‰, respectively, with relative standard deviations of less than 0.1‰ and 0.2‰, respectively. Therefore, the relative standard deviation of our $\delta^{13}C$ measurements is less than 0.2‰.

2.4. Temperature, salinity, nitrate and ammonium

Data on temperature, salinity, nitrate, and ammonium were provided by the Polar Research Center of China. Temperature and salinity were measured by the Seabird 911plus CTD system, with measurement accuracies of ± 0.01 °C and ± 0.0003 S/m (Siemens per meter, the unit of electrical conductivity), respectively. To ensure accuracy, the CTD sensors were calibrated before and after the voyage.

Seawater samples for nitrate and ammonium determination were filtered through 0.45 μm cellulose acetate membranes immediately after collection. Both ammonium and nitrate were measured in situ aboard the R/V *Xuelong 2*. Ammonium was determined using the spectrophotometric method of sodium hypobromite oxidation, while nitrate was determined using a nutrient automatic analyzer (AA3, SEAL Analytical GmbH) (GB/17378.4-2007). To ensure data reliability, parallel samples were collected from a random layer at each station for simultaneous analysis. The detection limits for nitrate and ammonium were 0.05 μmol/L and 0.020 μmol/L, respectively.

2.5. Chlorophyll-a

Size-fractionated chlorophyll-a was analyzed by the Second Institute of Oceanography, Ministry of Natural Resources of China, and provided by the Polar Research Center of China. Seawater samples were pre-filtered through a 200 μm sieve to remove most zooplankton. Subsequently, the pre-filtered samples were sequentially filtered through a 20 μm sieve, a 2 μm nucleopore membrane, and a GF/F Whatman filter. Chlorophyll-a on size-fractionated particles was measured by fluorescence after extraction with acetone (Holm-Hansen et al., 1965). Here, chlorophyll-a in the particles retained by the 20 μm sieve, the 2 μm nucleopore membrane, and the GF/F Whatman filter represent net-phytoplankton (Chla-Net), nano-phytoplankton (Chla-Nano) and pico-phytoplankton (Chla-Pico), respectively. The total chlorophyll-a (Chl-a) is the sum of Chla-Net, Chla-Nano, and Chla-pico. To express the proportion of smaller phytoplankton, $r_{smaller\ Chl\text{-}a}$ is defined as the ratio of the sum of Chla-Nano and Chla-Pico to the total Chl-a, as follows:

$$r_{smaller\ Chl-a} = \frac{Chla-Nano + Chla-Pico}{Chl-a} \times 100\% \quad (2)$$

3. Results

3.1. Temperature and salinity

The temperature in SSW varied from -1.78 °C to 0.42 °C, with an average of -0.94 °C. The sectional distribution of temperature showed lower surface temperatures near the coast and higher temperatures in the open ocean, with the highest values north of 65 °S at sections C3 and C4 (Fig. 2). Salinity in the SSW ranged from 33.46 to 34.15, with an average of 33.86, and was higher in the eastern section C9 (Fig. 3). The vertical variation of temperature and salinity indicated that the SML was about 25 m at sections C3 and C4 in the west and about 50 m at sections C8 and C9 in the east (Fig. 2 and Fig. 3), consistent with previous findings of the SML deepening from west to east (Wright et al., 2010).

The relationship between potential temperature and salinity indicates that water masses in our study area include SSW, WW, TCW, CDW and AABW (Fig.S1), with their characteristics listed in Table 1. The western Cosmonaut Sea, influenced by the thumb of the Weddell Gyre, exhibits higher temperature and lower salinity in the SSW. In contrast, the Cooperation Sea is affected by the northward transport of DSW, resulting in lower temperature and higher salinity in the SSW (Fig. 2 and Fig. 3). The DSW is produced by the mixing of cold ice shelf water (ISW) from the Emery Ice Shelf, which is exported northward and gradually rises to the surface driven by the Prydz Bay Gyre (Jia et al., 2022). The WW was located at a depth of approximately 50 m in our study area, with temperature ranging from -1.82 °C to -1.25 °C, the lower value being at section C4 (Fig. 2). Water at depths below 200 m at most sites exhibited high temperature and high salinity (T = 0.03−1.89 °C; S = 34.54−34.74), reflecting the influence of CDW. Exceptions occurred at the offshore sites of sections C4, C8 and C9, where temperatures below 200 m were less than 0.5 °C, indicating the influence of low-temperature DSW spreading northward (Fig. 2). The TCW is situated between WW and CDW at depths of 75 m to 150 m, with temperatures and salinities ranging from -1.82 °C to 1.74 °C and 34.10 to 34.60, respectively (Table 1). Additionally, the bottom water at sections C8 and C9 exhibited characteristics of AABW, with average temperature and salinity being -0.28 ± 0.19 °C and 34.66 ± 0.01, respectively, indicating the influence of AABW exported from the continental shelf (Table 1).

3.2. Nitrate and ammonium

Nitrate concentrations in SSW ranged from 14.68 to 31.37 μmol/dm^3 (mean 21.54 ± 4.88 μmol/dm^3), with the highest and lowest values observed at stations C4-05 and C4-07, respectively (Fig. 4). The sectional distribution of nitrate indicated the influence of CDW upwelling, characterized by high nitrate concentrations, particularly at sections C3, C4 and C9 near 64 °S, and section C8 near 65 °S. These upwellings lead to increased nitrate concentrations in the upper waters of these regions (Fig.4). Notably, waters above 150 m at the nearshore stations of sections C8 and C9 exhibited higher nitrate concentrations (Fig.4c, Fig.4d), corresponding to the northward export of shelf water, as indicated by temperature and salinity (Fig.2c, Fig.2d, Fig.3c, Fig.3d).

Ammonium concentrations in the SSW of sections C3 and C4 were below 0.4 μmol/dm^3, with maximum values occurring in the subsurface WW (Fig. 5). The formation of these ammonium subsurface maxima may be associated with the release and accumulation of ammonium during the degradation of organic matter in winter. In section C8, ammonium concentrations above 50 m were generally greater than 0.5 μmol/dm^3, possibly due to reduced phytoplankton uptake (Fig. 5c). In section C9, ammonium concentrations above 300 m, except at station C9-07, were below 0.3 μmol/dm^3 (Fig. 5d).

3.3. Size-fractionated Chl-a

The total Chl-a concentration in the SSW ranged from 0.08 μg/L to 2.36 μg/L, with the highest value recorded at a depth of 25 m at station C4-05 (Fig. 6a). Except for stations C4-02, C4-05, C8-02, and C9-03, the total Chl-a at the other stations was less than 0.40 μg/L, indicating a characteristic low phytoplankton biomass. The spatial distribution of total Chl-a showed higher concentrations near 64 °S at sections C3, C4, and C9, corresponding to the core area of CDW upwelling (Fig. 6a, Fig. 2). The upwelling brings nutrients such as nitrate and iron into the upper layer, promoting phytoplankton growth during the summer. It is noteworthy that no spatial correspondence between high Chl-a and upwelling was found in the previous BROKE-West study (Westwood et al., 2010).

The size-fractionated Chl-a data indicated the dominance of nano- and pico-phytoplankton in our study area. Except for stations C4-02, C4-

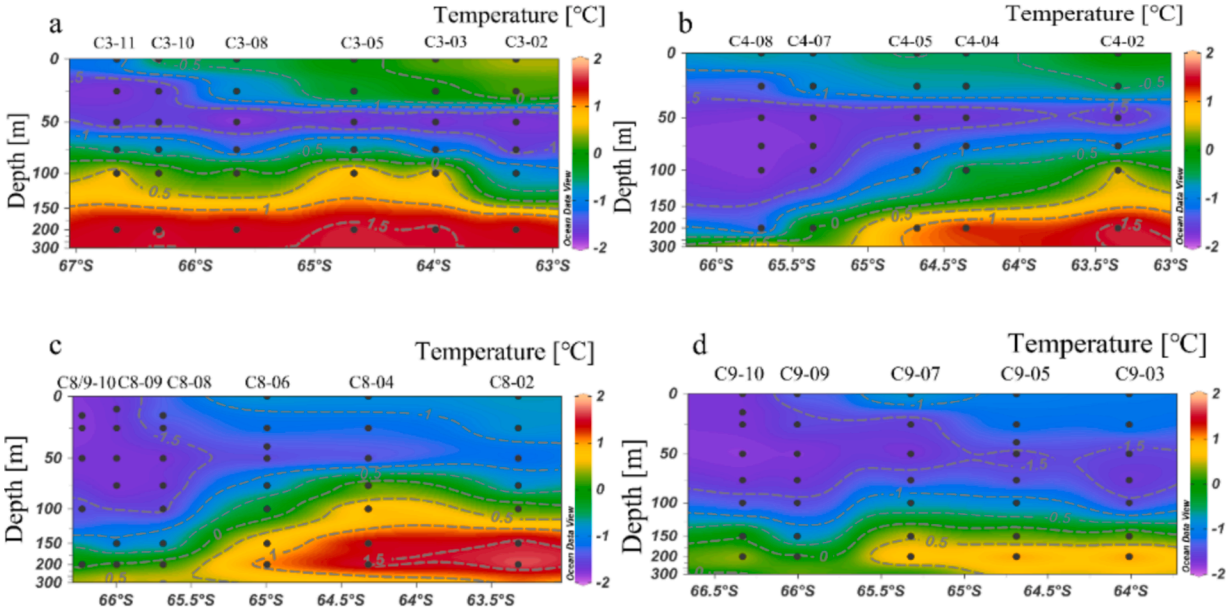

Figure 2. Meridional distribution of temperature in the upper 300 m water column at section C3 (a), section C4 (b), section C8 (c), and section C9 (d). The winter residual water (WW) was located at a depth of approximately 50 m at these sections, with temperatures ranging from -1.82 °C to -1.25 °C. At most sites, water below 200 m depth exhibited high temperatures, indicating the influence of CDW.

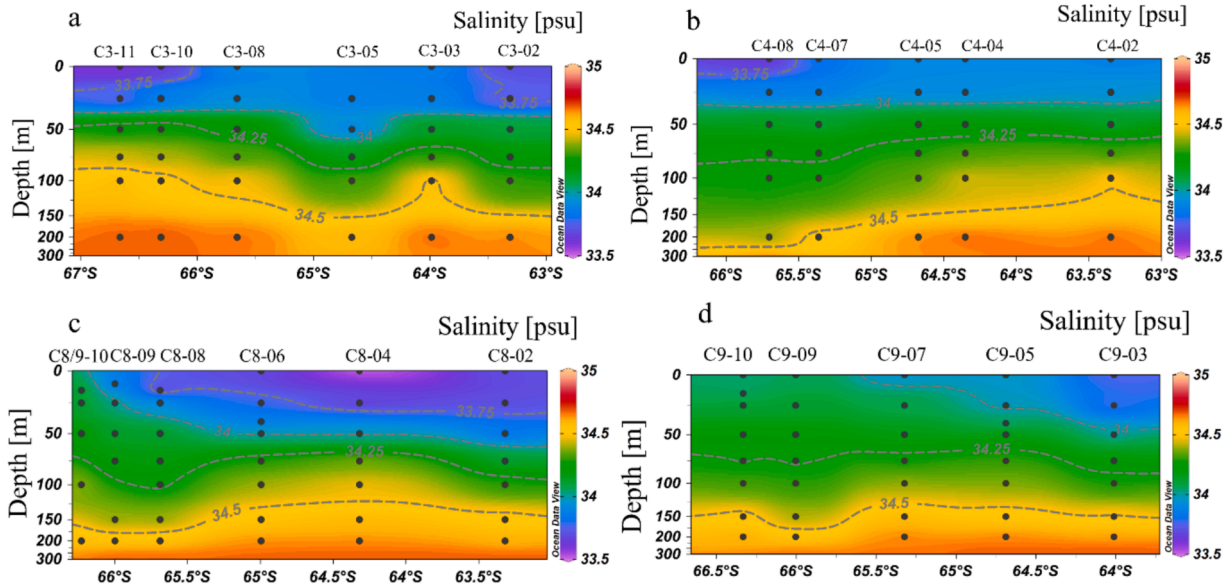

Figure 3. Meridional distribution of salinity in the upper 300 m water column at section C3 (a), section C4 (b), section C8 (c), and section C9 (d). At most sites, water below 200 m depth exhibited high salinity, indicating the influence of CDW.

Table 1
The range and average values of temperature, salinity, POC, and $\delta^{13}C_{POC}$ in various water masses. SSW, WW, TCW, CDW, and AABW denote summer surface water, winter residual water, thermocline water, circumpolar deep water and Antarctic bottom water, respectively. Note that the bottom water in sections C8 and C9 exhibited characteristics of AABW.

water mass	T (°C)		S (psu)		POC (μmol/dm^3)		δ^{13}C (‰)	
	range	avg	range	avg	range	avg	range	avg
SSW	-1.78 – 0.42	-0.94 ± 0.60	33.46 – 34.15	33.86 ± 0.16	1.13 – 15.73	6.68 ± 3.84	-31.1 – -26.6	-28.9 ± 1.0
WW	-1.82 – -1.25	-1.71 ± 0.12	33.81 – 34.28	34.12 ± 0.12	1.17 – 11.65	4.59 ± 2.66	-31.1 – -27.1	-29.2 ± 1.3
TCW	-1.82 – 1.74	-0.67 ± 1.10	34.10 – 34.60	34.36 ± 0.14	0.29 – 3.27	1.38 ± 0.71	-31.5 – -22.6	-27.6 ± 2.0
CDW	0.03 – 1.89	0.97 ± 0.55	34.54 – 34.74	34.67 ± 0.04	0.01 – 4.14	0.61 ± 0.60	-30.1 – -19.5	-24.5 ± 2.2
AABW	-0.49 – 0.13	-0.28 ± 0.19	34.64 – 34.67	34.66 ± 0.01	0.10 – 0.48	0.28 ± 0.11	-23.3 – -18.2	-21.8 ± 1.3

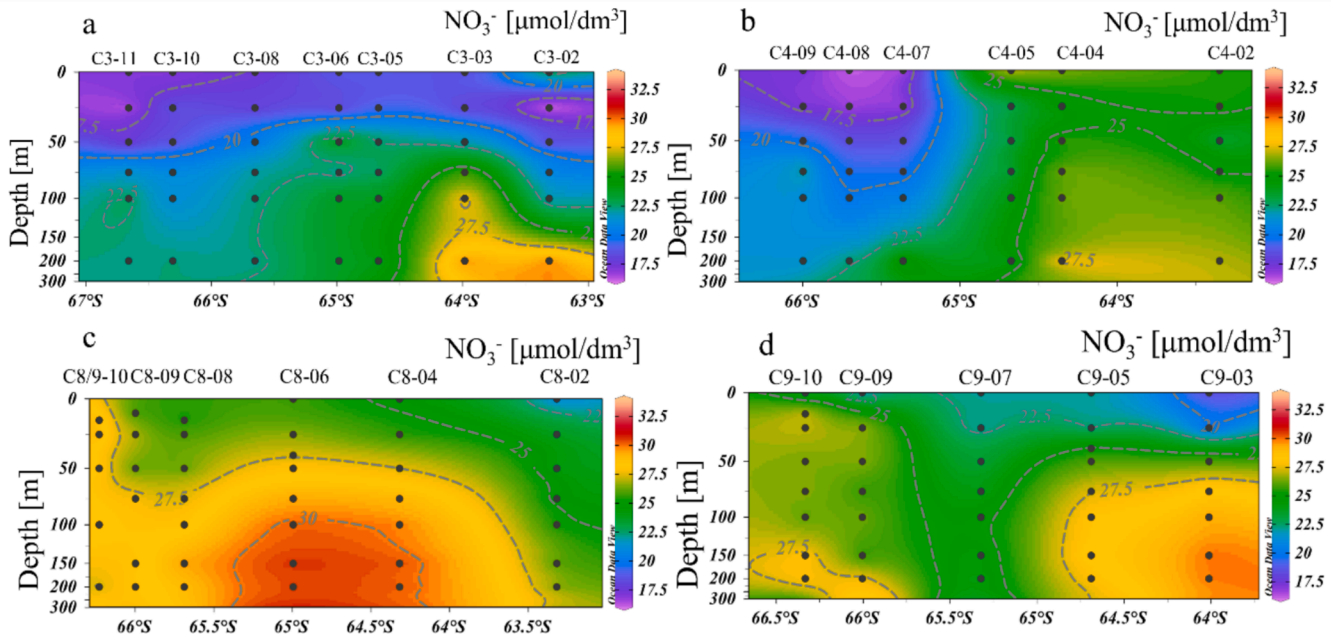

Figure 4. Meridional distribution of nitrate in the upper 300 m water column at section C3 (a), section C4 (b), section C8 (c), and section C9 (d).

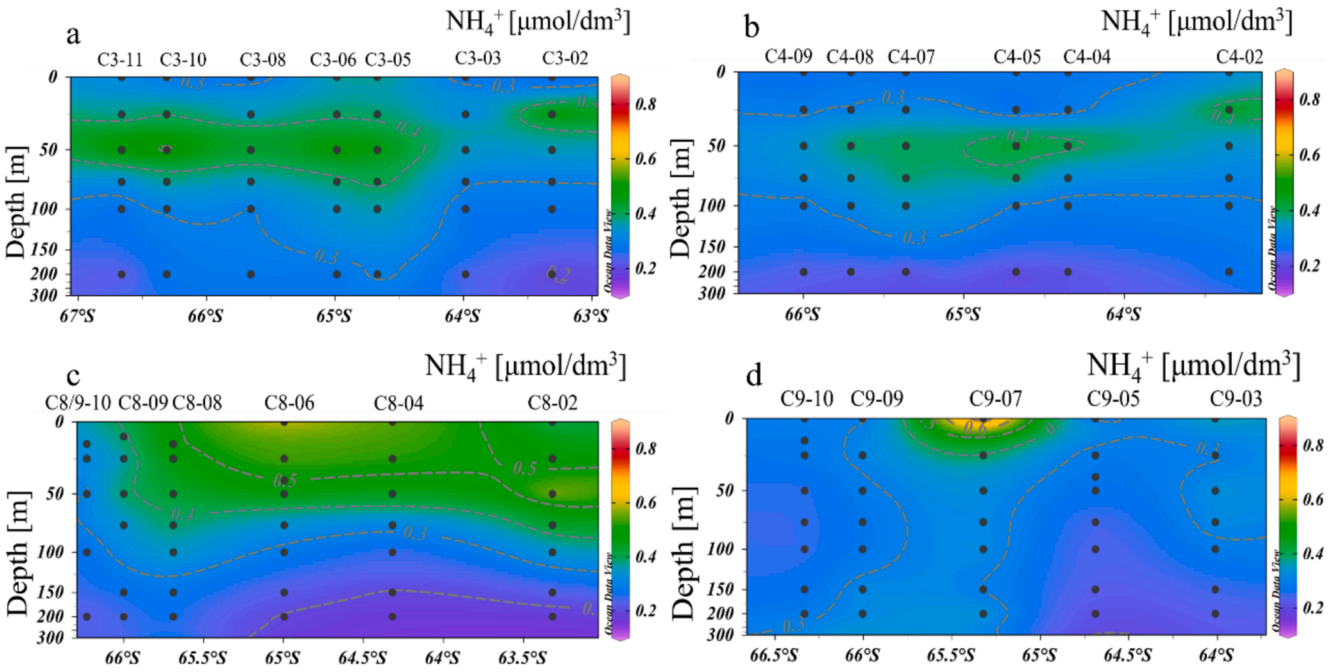

Figure 5. Meridional distribution of ammonium in the upper 300 m water column at section C3 (a), section C4 (b), section C8 (c), and section C9 (d).

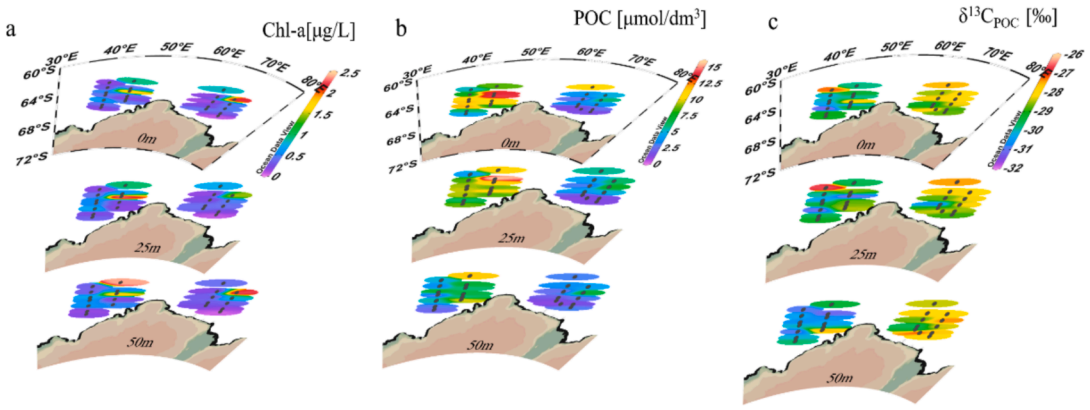

Figure 6. Spatial distribution of Chl-a (a), POC (b), and $\delta^{13}C_{POC}$ (c) at depths of 0 m, 25 m, and 50 m.

09, C9-03, C9-07 and C9-09, the average value of $r_{smaller\ Chl\text{-}a}$ in the water above 200 m at most stations was higher than 50%, with the highest value (77%) observed at station C4-07 (Fig. 7).

3.4. POC

The POC concentration in SSW ranged from 1.13 to 15.73 μmol/dm^3, with generally higher concentrations observed in the Cosmonaut Sea and lower concentrations in the Cooperation Sea (Fig. 6b). Compared to other regions, the POC concentrations in the 64−65 °S area of sections C3 and C4 were higher (9.32 − 15.73 μmol/dm^3), with the highest value observed at station C4-05, corresponding to higher Chl-a concentation (Fig. 6a, Fig. 6b). In comparison, the POC measurements in the Cosmonaut Sea were mostly higher than previously reported values (maximum 8.5 μmol/dm^3, Pasquer et al., 2010), but the values near the slopes of the Cooperation Sea (1.14−2.92 μmol/dm^3) were close to the lower limit of previous reports (1.6−18.7 μmol/L, Pasquer et al., 2010).

The POC profiles at all studied sites showed a decreasing trend with increasing depth. The most pronounced gradient of decrease occurred between the mixed layer and 200 m, with POC concentration below 200 m being lower than 1 μmol/dm^3 (Fig. S2). Specifically, the order of POC concentration in various water masses was as follows: SSW > WW > TCW > CDW > AABW. Notably, the POC concentration in AABW (0.28 ± 0.11 μmol/dm^3) was significantly lower than that in CDW (0.61 ± 0.60 μmol/dm^3) (Table 1).

3.5. C/N ratio

The average C/N molar ratio of particulate organic matter in the upper 50 m of the water column was 6.3 ± 2.1, closely aligning with the Redfield ratio of 6.6 (Redfield et al., 1963). The C/N ratios in the SSW of sections C3 and C4 were generally higher than those in sections C8 and C9. Specifically, the C/N ratios were greater than 10.0 at 0 m at stations C3-06 and C3-08, and at 25 m at stations C4-02 and C4-08, while at 0 m at stations C4-02 and C4-04, they were higher than 7.0. In contrast, the C/N ratios were less than 4.0 at 50 m at stations C3-10 and C3-11, and at 0 m and 25 m at station C8-06.

The distribution of C/N ratio in various sections exhibited a patchy pattern (Fig. S3). In section C3, the C/N ratios in the water column from 0 to 100 m at station C3-08 were higher than at other stations. In section C4, the C/N ratio was higher than in other sections, particularly at 200 m at station C4-04, where it reached 15.4. In section C8, the highest C/N

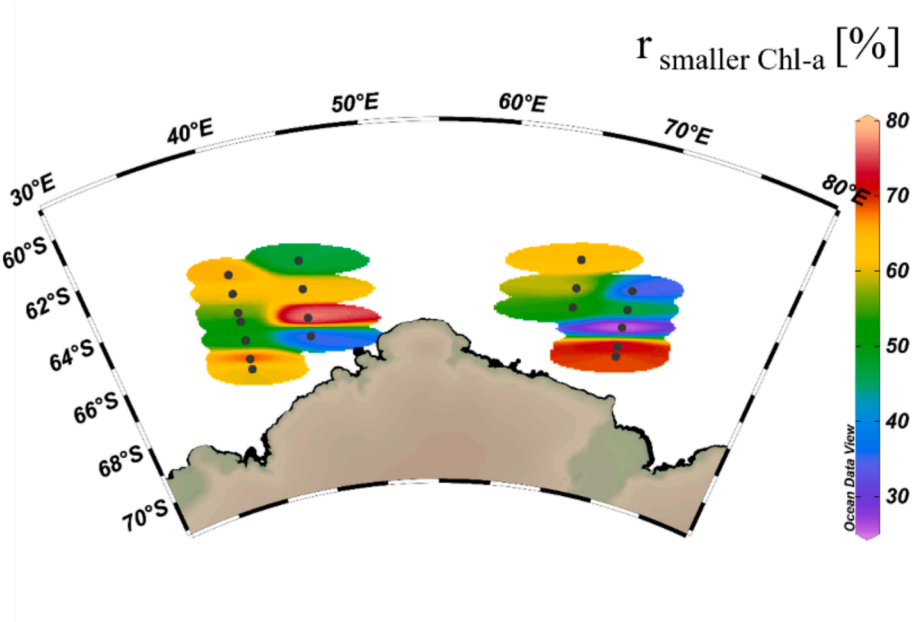

Figure 7. Spatial distribution of the integral means of $r_{smaller\ Chl\text{-}a}$ from 0 m to 200 m. The $r_{smaller\ Chl\text{-}a}$ is defined as the ratio of the sum of Chla-Nano and Chla-Pico to the total Chl-a.

ratio was observed at a depth of 75 m. In section C9, the C/N ratios in the water column at nearshore stations (such as C9-10) were usually higher than those at offshore stations (such as C9-05 and C9-03).

3.6. $\delta^{13}C_{POC}$

The spatial variation of $\delta^{13}C_{POC}$ in the SSW generally exhibited higher values in the east and lower values in the west, mirroring the distribution of POC (Fig. S2). The $\delta^{13}C_{POC}$ values in SSW ranged from -31.1‰ to -26.6‰, with an average of -28.9 ± 1.0‰. In WW, the $\delta^{13}C_{POC}$ values were not significantly different from those in SSW, with an average of -29.2 ± 1.3‰ (Table 1). The profiles of $\delta^{13}C_{POC}$ indicated an increase with depth below the WW, with average values of -27.6 ± 2.0‰ in TCW, -24.5 ± 2.2‰ in CDW, and -21.8 ± 1.3‰ in AABW (Table 1). Notably, $\delta^{13}C_{POC}$ values in AABW were significantly higher than those in CDW, corresponding to a significant decrease in POC (Table 1). The lowest $\delta^{13}C_{POC}$ value in our study area was -31.5‰, consistent with previous reports as low as -32% in the Southern Ocean (Tao et al., 2022).

4. Discussion

4.1. Effects of phytoplankton communities on $\delta^{13}C_{POC}$ in the SSW

Previous field and laboratory studies have indicated that temperature may influence $\delta^{13}C_{POC}$ by altering the concentration of dissolved CO_2 in seawater and the activity of carboxylases in phytoplankton. This results in a negative correlation between $\delta^{13}C_{POC}$ and $[(CO_2)_{aq}]$ in the mixed layer (Rau et al., 1989; Descolasgros and Fontugne, 1990). However, the presence of this negative correlation in the Southern Ocean remains uncertain and requires further investigation. Some studies suggest that $\delta^{13}C_{POC}$ variations in the Southern Ocean are influenced not only by $[(CO_2)_{aq}]$ but also by biological factors such as phytoplankton species, size, and growth rate (Kennedy and Robertson, 1995; Popp et al., 1999; Burkhardt et al., 1999; Henley et al., 2012). The situation in the Cosmonaut and Cooperation Seas is still unclear. This study focuses on the effect of phytoplankton size on the variation of $\delta^{13}C_{POC}$ in the mixed layer during summer.

Previous research has shown that the melting of sea ice in summer often creates a shallow mixed layer in the seasonal ice zones of the Southern Ocean. Here, phytoplankton, usually dominated by microdiatoms and *Phaeocystis antarctica*, contribute 25−67% of biological productivity (Smith and Asper, 2001; Davidson et al., 2010). Contrary to these scenarios, the average contribution of nano- and picophytoplankton to the total biomass ($r_{smaller\ chl\text{-}a}$) in the upper 200 m water column of the Cosmonaut Sea and the Cooperation Sea reached 57.7% and 50.9%, respectively, indicating an ecosystem dominated by smaller phytoplankton (Fig.7). In such an ecosystem, we found a significant positive correlation between $\delta^{13}C_{POC}$ in SSW and $r_{smaller\ Chl\text{-}a}$ (Fig.8) in both the Cosmonaut Sea and the Cooperation Sea, but not with temperature (figure not shown). This suggests that phytoplankton size influences the variation of $\delta^{13}C_{POC}$ in ecosystems dominated by small phytoplankton, and that $\delta^{13}C_{POC}$ increases with the biomass of smaller phytoplankton. This finding contrasts with previously reported diatom-dominated ecosystems, where smaller phytoplankton were associated with a larger isotopic fractionation factor, resulting in lower $\delta^{13}C_{POC}$

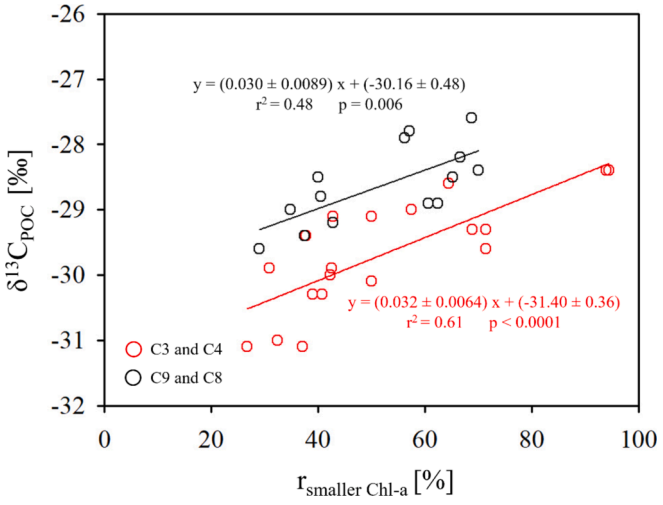

Figure 8. The relationship between $\delta^{13}C_{POC}$ and $r_{smaller\ Chl\text{-}a}$ in the SSW. The red circles represent the stations at sections C3 and C4 in the Cosmonaut Sea, and the black circles represent the stations at sections C8 and C9 in the Cooperation Sea.

values (Popp et al., 1999; Burkhardt et al., 1999). However, our results are consistent with observations in the control region of the SOIREE iron release experiments, where $\delta^{13}C_{POC}$ was 2–4‰ higher for pore sizes 5–70 μm than for >70 μm (Trull and Armand, 2001). Based on the intercepts of our fitted lines, the $\delta^{13}C_{POC}$ values for the larger net-phytoplankton in the Cosmonaut Sea and the Cooperation Sea were estimated to be -31.4 ± 0.4‰ and -30.2 ± 0.5‰, respectively (Fig.8). These lower $\delta^{13}C_{POC}$ values may be related to the species of phytoplankton. The dominant species in our study area are mainly central diatoms, pennate diatoms, and *Phaeocystis antarctica* (Davidson et al., 2010). The sizes of central diatoms, pennate diatoms, and *Phaeocystis antarctica* are > 20 μm, ~ 2 μm and 5−7 μm, respectively (Davidson et al., 2010; Kopczynska et al., 1995). Laboratory culture experiments showed that the fractionation effects of carbon isotopes in the assimilation of CO_2 and HCO_3^- by central diatoms are -20.9‰ and -29.9‰, respectively, while those of pennate diatoms are -16.9‰ and -26.0‰, respectively (Wong and Sackett, 1978). The greater isotope fractionation effect of central diatoms leads to lower $\delta^{13}C_{POC}$ values, which may explain the lower $\delta^{13}C_{POC}$ values of net-phytoplankton in the Cosmonaut Sea and the Cooperation Sea. Therefore, the observed increase in $\delta^{13}C_{POC}$ values with increasing $r_{smaller\ Chl\text{-}a}$ in the Cosmonaut Sea and the Cooperation Sea might be explained by an increase in the abundance of pennate diatoms and a decrease in central diatoms.

The effect of phytoplankton size and species on $\delta^{13}C_{POC}$ is also evident in the relationship between $\delta^{13}C_{POC}$ and POC content in smaller particles in our study area. We found a significant positive linear correlation between POC and Chl-a in SSW of all sections except section C4. The linear fitting equations of sections C3, C8 and C9 are as follows: POC (μmol/L) = (11.76 ± 2.61) · Chl-a (μg/L) + (3.56 ± 1.12) (r^2 = 0.63, p = 0.0007) (section 3); POC (μmol/L) = (7.48 ± 2.25) · Chl-a (μg/L) + (1.09 ± 0.86) (r^2 = 0.44, p = 0.005) (section 8); and POC (μmol/L) = (8.34 ± 2.20) · Chl-a (μg/L) + (1.10 ± 0.91) (r^2 = 0.677, p = 0.07) (section 9)(Fig.9). The positive correlation between POC and Chl-a suggests that fresh biogenic organic matter was the primary factor influencing POC variations in our study area.

Notably, no positive correlation between POC and Chl-a was observed in section C4, mainly due to the influence of station C4-05, which had higher Chl-a concentrations but lower POC contents. The anomalies at station C4-05 may be related to changes in phytoplankton community composition. Davidson et al (2010) noted that the cellular carbon content of *Phaeocystis antarctica* in the 30−80 °E seasonal ice zone is much lower than that of diatoms, which have higher cellular carbon contents. Therefore, although we lack direct evidence, the abnormally low cellular carbon content at station C4-05 may be due to a greater abundance of *Phaeocystis antarctica*.

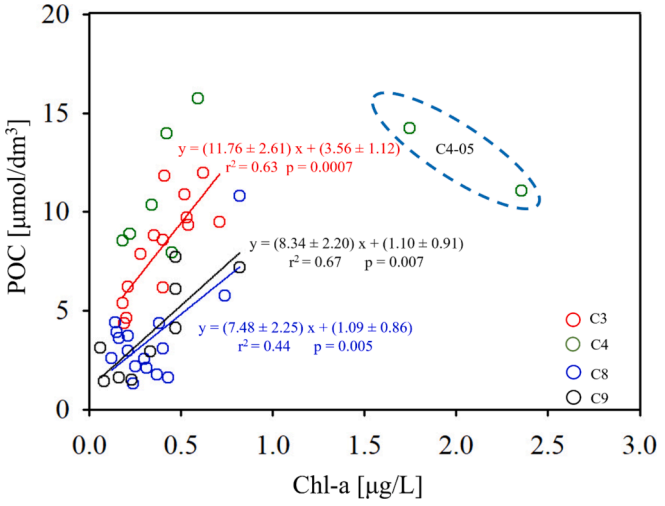

Figure 9. The relationship between Chl-a and POC in the SSW. Red, blue, and black circles represent samples from sections C3, C8, and C9, respectively. Green circles indicate samples from section C4. Blue dotted circles denote samples collected at depths of 0 m and 25 m at station C4-05.

For the fitting relationships in sections C3, C8, and C9, the intercept represents the detrital POC content. The detrital POC content in the SSW of section C3 (3.56 ±1.12 μmol/dm^3) is higher than that in sections C8 and C9 (1.09 ± 0.86 and 1.10 ± 0.91 μmol/dm^3, respectively). Assuming the detrital POC content was constant in each section, the biogenic POC (bPOC) was estimated by subtracting the intercept from the POC measurement. Further assuming that the partitioning of bPOC in smaller and larger particles is the same as that of Chl-a, the concentration of biogenic POC in smaller particles was estimated by the following equation:

$$bPOC_{smaller} = bPOC \cdot r_{smaller\ Chl-a} \quad (2)$$

where $bPOC_{smaller}$ represents organic carbon content in the smaller biogenic particles (μmol/dm^3), bPOC represents total biogenic organic carbon content (μmol/dm^3), and $r_{smaller\ Chl\text{-}a}$ represents the contribution of nano- and pico-phytoplankton to the total biomass (%).

Our estimates indicate that $bPOC_{smaller}$ in the SSW of the Cosmonaut Sea and the Cooperation Sea ranged from 0.33 to 3.21 μmol/dm^3 and 0.17 to 4.49 μmol/dm^3, respectively, accounting for 32–71% and 25–75% of the bPOC. The proportion of smaller POC in the Cosmonaut Sea was slightly lower than that in the Cooperation Sea, possibly reflecting differences in the composition of phytoplankton communities.

Interestingly, the relationship between $\delta^{13}C_{POC}$ and $bPOC_{smaller}$ differed between the Cosmonaut Sea and the Cooperation Sea, showing a negative correlation in the former and a positive correlation in the latter (Fig. 10). This discrepancy may reflect variations in isotope fractionation due to the distinct species of smaller phytoplankton in the SSW of these two seas. Phytoplankton community composition from the same voyage indicates that smaller phytoplankton in sections C8 and C9 of the Cooperation Sea are dominated by pennate diatoms, while in section C3 of the Cosmonaut Sea, *Phaeocystis antarctica* and pennate diatoms are predominant. Changes in the C/N ratio in particulate organic matter also indicate differences in phytoplankton species between the two seas. Our results showed that the C/N ratio in the SSW of the Cosmonaut Sea is higher than in the Cooperation Sea (Fig. S3), likely reflecting the lower C/N ratios associated with the efficient nitrogen uptake by diatoms under nutrient-rich conditions (Martiny et al., 2013). In contrast, the cysts of *Phaeocystis antarctica* are primarily composed of polysaccharides with a high C/N ratio (Davidson et al., 2010; Pasquer et al., 2010). Therefore, in the SSW of the Cooperation Sea, increased pennate diatom biomass and enhanced photosynthesis result in more $bPOC_{smaller}$ and heavier carbon isotopic compositions due to the absorption of more dissolved CO_2, leading to a positive correlation between $\delta^{13}C_{POC}$ and $bPOC_{smaller}$ (Fig.10b). This positive correlation between $\delta^{13}C_{POC}$ and POC, driven by photosynthetic mechanisms (Rau et al., 1989), aligns with previous findings in Prydz Bay (Kopczynska et al., 1995; Zhang et al., 2014; Ren et al., 2015) and the 40–53 °S region of the Southern Ocean (Soares et al., 2020). Unlike the Cooperation Sea, the negative correlation between $\delta^{13}C_{POC}$ and $bPOC_{smaller}$ in section C3 of the Cosmonaut Sea is not explained by photosynthetic mechanisms but may be due to changes in species among smaller phytoplankton and their different isotope effects (Fig. 10a). Laboratory studies have shown that *Phaeocystis antarctica* exhibits greater carbon isotope fractionation when assimilating inorganic carbon (fractionation factors for CO_2 and HCO_3^- absorption are -26.4‰ and -35.5‰, respectively) compared to diatoms, resulting in a lower $\delta^{13}C$ value in the synthesized organic matter (Wong and Sackett, 1978; Kopczynska et al., 1995). This indicates that as the abundance of *Phaeocystis antarctica* relative to pennate diatoms increases in the smaller phytoplankton of the Cosmonaut Sea, the $\delta^{13}C$ value in the total POC decreases. Notably, the $\delta^{13}C_{POC}$ in section C3 of the Cosmonaut Sea is significantly lower than that in sections C8 and C9 of the Cooperation Sea (Fig. 6c), which cannot be attributed to the

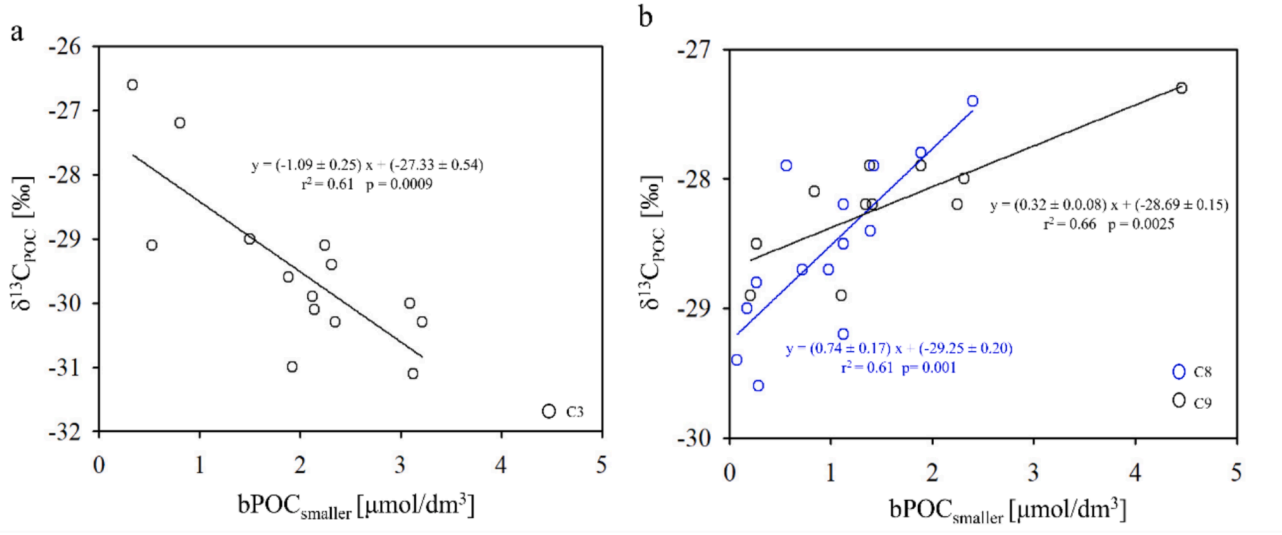

Figure 10. Relationship between $\delta^{13}C_{POC}$ and $bPOC_{smaller}$ in SSW of the Cosmonaut Sea (a) and the Cooperation Sea (b). In subgraph (a), black circles denote samples from section C3. In subgraph (b), blue and black circles represent samples from sections C8 and C9, respectively.

isotope effect of central and pennate diatoms. Thus, changes in species among smaller phytoplankton may explain the negative correlation between $\delta^{13}C_{POC}$ and $bPOC_{smaller}$ in section C3 of the Cosmonaut Sea.

4.2. Isotope fractionation in the remineralization of particulate organic matter

Below the SSW in the Cosmonaut and Cooperation Seas, the POC content and $\delta^{13}C_{POC}$ gradually decreased and increased with depth, respectively, reflecting the effect of organic matter remineralization on POC and its isotopic composition (Fig. S2). During the settling of particulate organic matter, POC was gradually degraded and converted into dissolved CO_2, with ^{12}C being preferentially released. This process results in a continuous enrichment of ^{13}C in the residual particulate organic matter (Trull et al., 2008). For example, the rapid degradation of amino acids and carbohydrates in middle and deep waters leads to the accumulation of ^{13}C in the residual POC, although some ^{12}C-enriched, non-degradable lipids remain (Eadie and Jeffrey, 1973; Cavagna et al., 2013; Schmittner et al., 2013). Contrary to this general trend, a few studies have observed a decrease in $\delta^{13}C_{POC}$ with depth, attributing it to changes in the organic composition of sinking particulate organic matter (Cavagna et al., 2013; Close and Henderson, 2020). The observed changes in POC and $\delta^{13}C_{POC}$ in the Cosmonaut and Cooperation Seas followed typical vertical distributions, indicating that the remineralization of particulate organic matter is the the primary factor controlling the isotopic composition changes in the middle and deep waters. Unfortunately, few studies to date have assessed carbon isotope effects in the remineralization of particulate organic matter in the Southern Ocean. Here, a Rayleigh model is employed to address this gap.

Assuming that the POC in mid-deep water is entirely derived from the export of biogenic POC in the upper water and that the isotopic fractionation coefficient is constant during the remineralization of particulate organic matter, the change in $\delta^{13}C_{POC}$ in mid-deep water can be described as follows (Mariotti et al., 1981; Freudenthal et al., 2001):

$$\delta^{13}C_{residual\ POC} = \delta^{13}C_{initial\ POC} - \varepsilon \cdot \ln f \quad (3)$$

where $\delta^{13}C_{initial\ POC}$ and $\delta^{13}C_{residual\ POC}$ represent the carbon isotopic composition of the initial particulate organic matter input into the mid-deep water and the carbon isotopic composition of the residual organic matter after remineralization (i.e., the measured $\delta^{13}C_{POC}$ in the mid-deep water), respectively. ε denotes the fractionation coefficient of carbon isotopes during the remineralization of particulate organic matter. The term f represents the fraction of the residual POC to initial POC. Here, f is estimated by dividing the measured POC at each depth below 50 m by the maximum POC in the entire water column (occurring at 0 or 25 m). This estimate has certain uncertainties. For example, POC in upper waters will remineralize and may not all settle to deep water, and upwelling and lateral transport may lead to POC in deep water not being entirely derived from biogenic POC in upper water. However, in the study area where biogenic particle deposition is dominant, the estimated f approximates the fraction of POC that is not degraded. Our results show a significant linear negative correlation between $\delta^{13}C_{POC}$ and ln$f$ in both the Cosmonaut Sea and the Cooperation Sea. The slopes of the fitted lines indicate that the fractionation coefficients of carbon isotopes during remineralization are 1.5 ± 0.2‰ and 1.6 ± 0.2‰ in the Cosmonaut Sea and in the Cooperation Sea, respectively (Fig. 11). The small fractionation coefficient implies little change in carbon isotopic composition during the degradation of particulate organic matter, which is consistent with our observed small difference in $\delta^{13}C_{POC}$ between TCW and CDW (Table 1). The small isotope effect also suggests that the carbon isotope signal in the upper waters can be well preserved in deep water, thus providing the possibility for reconstructing changes in paleoproductivity (Bentaleb et al., 1996; Fischer, et al., 1998; Combes et al., 2008). For comparison, the difference in $\delta^{13}C_{POC}$ in settling particles in the upper and deep waters of Ryder Bay and Marguerite Bay in the Antarctic Peninsula was only 0.4‰ (Henley et al., 2012). The $\delta^{13}C_{POC}$ in the small-sized POC (1 - 53 μm) varied only 1‰ to 2‰ in the mid-deep waters of the Atlantic section of the Southern Ocean (Cavagna et al., 2013). Similarly, Fischer et al. (1997) found that the difference of $\delta^{13}C$ in plankton and sinking particulate organic matter in the upper Atlantic Ocean was less than 2‰. In contrast, some studies have shown that carbon isotopes have larger fractionation coefficients during the degradation of organic matter. For example, $\delta^{13}C$ values in large-sized POC (> 53 μm) and some organic components (cholesterol and brassicosterol) in the Atlantic section of the Southern Ocean increased by 2−5‰ with depth (Cavagna et al., 2013). The $\delta^{13}C_{POC}$ difference between sinking particulate organic matter and surface sediments reaches 0.5-3.2‰ in the tropical-subtropical Atlantic Ocean and 3.0‰ in the Southern Ocean (Fischer et al.,1998). Additionally, the fractionation coefficient of carbon isotopes of easily degradable organic matter in subtropical eastern Atlantic sediments during early diagenesis was estimated to be 4.39‰ (Freudenthal et al., 2001). The larger isotope effect means that the $\delta^{13}C$ of the sedimentary organic matter differs from that of the source organic matter, leading to a deviation from the upper marine ecosystem. Therefore, the fractionation effect of carbon isotopes

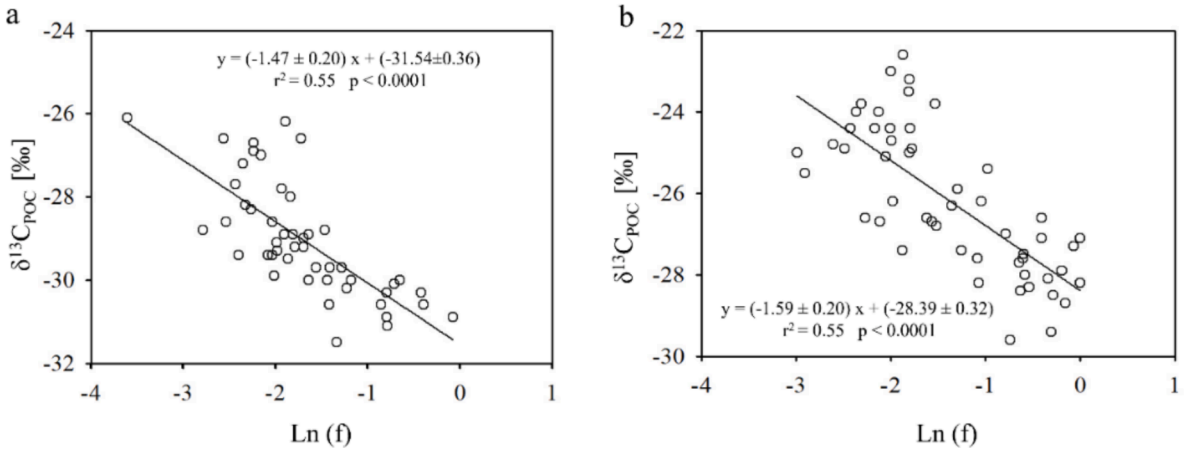

Figure 11. The relationship between $\delta^{13}C_{POC}$ and ln(f) in WW, TCW, and CDW of the Cosmonaut Sea (a) and the Cooperation Sea (b). Here, f represents the fraction of residual POC relative to the initial POC entering the deep water.

during remineralization in different sea areas may be related to changes in the size and composition of organic matter, as well as the microbial species involved.

4.3. Bottom $\delta^{13}C_{POC}$ as an indicator of AABW formation

The $\delta^{13}C_{POC}$ values in the bottom water of sections C8 and C9 in the Cooperation Sea are unusually high, ranging from -23.3‰ to -18.2‰, with an average of -21.8 ± 1.3‰ (Table 1). These values cannot be explained by the remineralization of particulate organic matter in the water column, suggesting input from other sources with high $\delta^{13}C$ characteristics. Previous studies have reported $\delta^{13}C_{POC}$ values of -21.9 ± 3.0‰ in intact ice, -19.9 ± 3.0‰ in layered floating ice, and -20.1 ± 2.2‰ at ice-water interfaces in the Weddell Sea, and $\delta^{13}C_{POC}$ values ranging from -15‰ to -8‰ in ice cores from Prydz Bay (Gibson et al., 1999). These elevated $\delta^{13}C_{POC}$ values reflect the influence of ice algae under limited supplies of dissolved carbon dioxide and nitrate within the ice mass (Kennedy et al., 2002). Numerous studies have shown that the loose structure of ice provides nutrients for ice algae growth, promoting the formation of high-abundance communities at the bottom of ice shelves (Arrigo et al., 1995; Van Leeuwe et al., 2018). The biomass of ice algae communities at the bottom of ice shelves accounts for 44.2% of the total biomass in the ice environment of East Antarctica (McMinn et al., 2007). Therefore, ice algae may be a source of particulate organic matter with high $\delta^{13}C_{POC}$ characteristics in the Cooperation Sea. However, the transport mechanism of this ^{13}C-enriched particulate organic matter from ice algae to bottom waters remains unclear. The formation of AABW in the Cape Darnley polynya may play a crucial role in this transport. Previous studies have shown that DSWs produced by sea ice formation in the Cape Darnley polynya mix with rising CDWs to form AABWs, which descend along the continental slope and enter the bottom of the open ocean, being transported westward to 68 °E and northward to 65.5 °S (Pu, 2002; Ohshima et al., 2013; Jia et al., 2022). The sites with high $\delta^{13}C_{POC}$ characteristics in the bottom water observed in this study fall within the AABW influence area. Therefore, ice algae released from ice shelves are likely to affect bottom waters in our study area through AABW transport. Several studies have confirmed that ice algae exported from ice shelves provide food for zooplankton and benthic organisms in the open ocean (Liu et al., 2021; Van Leeuwe et al., 2018), supporting the claim that some organic matter in bottom water is contributed by ice algae.

Assuming that the particulate organic matter in the bottom water of the Cooperation Sea originates from the sinking of local phytoplankton organic matter and the horizontal transport of ice algae organic matter, the following mass balance equations can be established:

$$f_{local} + f_{ice\ algae} = 1 \quad (4)$$

$$f_{local} \cdot \delta^{13}C_{POC,local} + f_{ice\ algae} \cdot \delta^{13}C_{POC,ice\ algae} = \delta^{13}C_{POC} \quad (5)$$

where f_{local} and $f_{ice\ algae}$ represent the fractional contribution of POM from local deposition and ice algae, respectively; $\delta^{13}C_{POC,\ local}$ and $\delta^{13}C_{POC,\ ice\ algae}$ represent the characteristic $\delta^{13}C$ values in POM from local deposition and ice algae, respectively; $\delta^{13}C_{POC}$ represents the measured carbon isotopic composition of particulate organic matter in the bottom water of the Cooperation Sea. To estimate the contributions of the two sources, the values of $\delta^{13}C_{POC,\ local}$ and $\delta^{13}C_{POC,\ ice\ algae}$ were taken as the average $\delta^{13}C_{POC}$ in the CDW of the Cooperation Sea and the average $\delta^{13}C_{POC}$ in an ice core collected from the Amery Ice Shelf during the same voyage, which were -23.6‰ and -12.4‰, respectively. Our estimates indicate that the contributions of ice algae-derived and locally deposited POM to POC in the bottom water of the Cooperation Sea ranged from 6% to 48% and from 52% to 94%, with averages of 16% and 84%, respectively (Table 2). Except for station C8-04, the f_{local} values in water within 60 m from the seabed ranged from 81% to 94%, indicating that local deposition plays a dominant role in the source of POM in the AABW of the Cooperation Sea. The variation of $f_{ice\ algae}$ values in the water within 60 m from the seabed shows that it is higher than 9% south of 65.5 °S and less than 8% north of 65.0 °S, demonstrating a general trend of decreasing from the continental shelf (Fig. S4). This spatial variation indicates the influence of ice algae organic matter sources and AABW transport pathways. The presence of horizontally transported ice algal organic matter in bottom waters suggests that $\delta^{13}C_{POC}$ in sediments may not fully represent local productivity. Further studies are required to elucidate the spatial variability of ice algal organic matter in Southern Ocean sediments.

5. Conclusion

This study examines the spatial variability of POC and $\delta^{13}C_{POC}$ in the Cosmonaut and Cooperation Seas during summer. POC concentrations decreased with depth, while $\delta^{13}C_{POC}$ generally increased, indicating diverse biogeochemical processes across different water masses. In the upper SSW of both seas, $\delta^{13}C_{POC}$ was positively correlated with the proportion of small-sized Chl-a, suggesting that the photosynthesis of small-sized phytoplankton primarily influenced $\delta^{13}C_{POC}$. However, species-specific differences among small-sized phytoplankton led to a negative correlation between $\delta^{13}C_{POC}$ and $bPOC_{smaller}$ in the Cosmonaut Sea (dominated by *Phaeocystis antarctica*), and a positively correlation in the Cooperation Sea (dominated by pennate diatoms). This highlights that phytoplankton species also impact $\delta^{13}C_{POC}$ changes. In deeper WW,

Table 2
POC, $\delta^{13}C_{POC}$, and the estimated f_{local} and $f_{ice\ algae}$ in the AABW near the Cape Darnley polynya in the Cooperation Sea. The f_{local} and $f_{ice\ algae}$ represent the contribution fractions of POM from local deposition and ice algae, respectively.

Station	Longitude (°E)	Latitude (°S)	Bottom depth (m)	Sampling depth (m)	POC (μmol/dm^3)	$\delta^{13}C_{POC}$ (‰)	f_{local} (%)	$f_{ice\ algae}$ (%)
C9-03	69.03	64.01	3319	3000	0.15	-21.7	83	17
				3292	0.19	-22.9	94	6
C9-07	68.94	65.32	2764	2734	0.27	-22.4	89	11
C9-09	68.98	66.00	2352	1850	0.36	-22.7	92	8
				2320	0.29	-22.6	91	9
C9-10	69.01	66.33	2020	1990	0.28	-22.4	89	11
C8-04	65.02	64.32	3700	3000	0.21	-21.1	78	22
				3670	0.29	-18.2	52	48
C8-06	65.00	65.00	3169	3110	0.1	-22.7	92	8
C8-08	64.91	65.69	2836	2806	0.26	-21.5	81	19

TCW, and CDW water masses, $\delta^{13}C_{POC}$ decreased with an increasing residual POC fraction, reflecting the remineralization effect of particulate organic matter. The carbon isotope fractionation coefficients during remineralization in the Cosmonaut Sea and the Cooperation Sea were estimated using the Rayleigh model to be 1.5 ± 0.2‰ and 1.6 ± 0.2‰, respectively. These small isotope effects indicate that remineralization does not significantly alter the carbon isotopic composition of biogenic organic matter from the upper ocean. Additionally, abnormally high $\delta^{13}C_{POC}$ values were observed in the bottom water outside Cape Darnley polynya in the Cooperation Sea. These values cannot be fully explained by the local export of upper POM and its isotope fractionation but are likely supplemented by ice algae organic matter transported by AABW. A simple isotopic mass balance estimate suggests that 6–19% of the POC in the AABW of the Cooperation Sea is contributed by ice algae organic matter transported from the continental shelf. Consequently, the potential impact of phytoplankton communities and AABW transport should be considered when applying $\delta^{13}C_{POC}$ in sediments to reconstruct paleoproductivity in the Southern Ocean.

CRediT authorship contribution statement

Jiawen Kang: Writing – original draft, Visualization, Methodology, Formal analysis. **Qiang Hao:** Validation, Methodology, Formal analysis. **Shunan Cao:** Investigation, Data curation. **Jun Zhao:** Validation, Methodology, Formal analysis. **Zifei Yang:** Methodology, Investigation. **Zhen Tang:** Investigation. **Minfang Zheng:** Validation, Resources, Methodology. **Yusheng Qiu:** Software, Data curation. **Mengya Chen:** Validation, Resources. **Jianming Pan:** Writing – review & editing, Funding acquisition. **Jianfeng He:** Writing – review & editing, Project administration, Conceptualization. **Min Chen:** Writing – review & editing, Supervision, Investigation, Funding acquisition, Conceptualization.

Declaration of competing interest

The authors declare that they have no known competing financial interests or personal relationships that could have appeared to influence the work reported in this paper.

Data availability

Data will be made available on request.

The data supporting the findings of this study are available in the supplementary information dataset.

Acknowledgements

We are grateful to the National Polar Science Data Center of China for providing data on temperature, salinity, nutrients and Chl-a. This work was supported by Polar Research Institute of China (IRASCC 02-01-01, IRASCC 01-01-02C) and National Natural Science Foundation of China (No. 41721005).

Appendix A. Supplementary data

Supplementary data to this article can be found online at https://doi.org/10.1016/j.pocean.2024.103363.

Appendix C. Supplementary data

Supplementary data to this article can be found online at https://doi.org/10.1016/j.pocean.2024.103363.

References

Arrigo, K.R., Dieckmann, G., Gosselin, M., et al., 1995. High resolution study of the platelet ice ecosystem in McMurdo Sound, Antarctica: Biomass, nutrient, and production profiles within a dense microalgal bloom. Mar. Ecol. Prog. Ser. 127 (1–3), 255–268. https://doi.org/10.3354/meps127255.

Arrigo, K.R., Lowry, K.E., van Dijken, G.L., 2012. Annual changes in sea ice and phytoplankton in polynyas of the Amundsen Sea, Antartica. Deep-Sea Res. II 71–76, 5–15. https://doi.org/10.1016/j.dsr2.2012.03.006.

Arrigo, K.R., van Dijken, G.L., Strong, A.L., 2015. Environmental controls of marine productivity hot spots around Antarctica. J. Geophys. Res. Oceans 120 (8), 5545–5565. https://doi.org/10.1002/2015JC010888.

Benner, R., Amon, R.M.W., 2015. The size-reactivity continuum of major bioelements in the ocean. Ann. Rev. Mar. Sci. 7, 185–205. https://doi.org/10.1146/annurev-marine-010213-135126.

Bentaleb, I., Fontugne, M., Descolas-Gros, C., et al., 1996. Organic carbon isotopic composition of phytoplankton and sea-surface pCO_2 reconstructions in the Southern Indian Ocean during the last 50000 yr. Org Geochem. 24 (4), 399–410. https://doi.org/10.1016/0146-6380(96)00043-5.

Bentaleb, I., Fontugne, M., Descolas-Gros, C., et al., 1998. Carbon isotopic fractionation by plankton in the Southern Indian Ocean: Relationship between $\delta^{13}C$ of particulate organic carbon and dissolved carbon dioxide. J. Mar. Syst. 17 (1–4), 39–58. https://doi.org/10.1016/S0924-7963(98)00028-1.

Bindoff, N.L., Rosenberg, M.A., Warner, M.J., 2000. On the circulation and water masses over the Antarctic continental slope and rise between 80 and 150 °E. Deep-Sea Res. II 47, 2299–2326. https://doi.org/10.1016/S0967-0645(00)00038-2.

Burkhardt, S., Riebesell, U., Zondervan, I., 1999. Effects of growth rate, CO_2 concentration, and cell size on the stable carbon isotope fractionation in marine phytoplankton. Geochim. Cosmochim. Acta 63 (22), 3729–3741. https://doi.org/10.1016/S0016-7037(99)00217-3.

Cavagna, A.J., Dehairs, F., Bouillon, S., et al., 2013. Water column distribution and carbon isotopic signal of cholesterol, brassicasterol and particulate organic carbon in the Atlantic sector of the Southern Ocean. Biogeosciences 10 (4), 2787–2801. https://doi.org/10.5194/bg-10-2787-2013.

Close, H.G., Henderson, L.C., 2020. Open-ocean minima in $\delta^{13}C$ values of particulate organic carbon in the lower euphotic zone. Front. Mar. Sci. 7. https://doi.org/10.3389/fmars.2020.540165.

Combes, H.J., Esper, O., De La Rocha, C.L., et al., 2008. Diatom $\delta^{13}C$, $\delta^{15}N$, and C/N since the Last Glacial Maximum in the Southern Ocean: Potential impact of species composition. Paleoceanography 23 (4). https://doi.org/10.1029/2008PA001589.

Comiso, J.C., Gordon, A.L., 1996. Cosmonaut polynya in the Southern Ocean: structure and variability. J. Geophys. Res. 101, 18297–18313. https://doi.org/10.1029/96JC01500.

Davidson, A.T., Scott, F.J., Nash, G.V., et al., 2010. Physical and biological control of protistan community composition, distribution and abundance in the seasonal ice zone of the Southern Ocean between 30 and 80 °E. Deep-Sea Res. II 57 (9–10), 828–848. https://doi.org/10.1016/j.dsr2.2009.02.011.

Dehairs, F., Kopczynska, E., Nielsen, P., et al., 1997. $\delta^{13}C$ of Southern Ocean suspended organic matter during spring and early summer: Regional and temporal variability. Deep-Sea Res. II 44 (1–2), 129–142. https://doi.org/10.1016/s0967-0645(96)00073-2.

Descolasgros, C., Fontugne, M., 1990. Stable carbon isotope fractionation by marine phytoplankton during photosynthesis. Plant Cell Environ. 13 (3), 207–218. https://doi.org/10.1111/j.1365-3040.1990.tb01305.x.

Eadie, B.J., Jeffrey, L.M., 1973. $\delta^{13}C$ analyses of oceanic particulate organic matter. Mar. Chem. 1, 199–209. https://doi.org/10.1016/0304-4203(73)90004-2.

Fabiano, M., Povero, P., Danovaro, R., 1996. Particulate organic matter composition in Terra Nova bay (Ross Sea, Antarctica) during summer 1990. Antarct. Sci. 8 (1), 7–13. https://doi.org/10.1017/s095410209600003x.

Fischer, G., Schneider, R., Muller, P.J., et al., 1997. Anthropogenic CO_2 in Southern Ocean surface waters: Evidence from stable organic carbon isotopes. Terra Nova 9 (4), 153–157. https://doi.org/10.1046/j.1365-3121.1997.d01-29.x.

Fischer, G., Müller, P.J., Wefer, G., 1998. Latitudinal $\delta^{13}C_{org}$ variations in sinking matter and sediments from the South Atlantic: effects of anthropogenic CO_2 and implications for paleo-pCO_2 reconstructions. J. Mar. Syst. 17 (1–4), 471–495. https://doi.org/10.1016/S0924-7963(98)00059-1.

Freudenthal, T., Wagner, T., Wenzhöfer, F., et al., 2001. Early diagenesis of organic matter from sediments of the eastern subtropical Atlantic: Evidence from stable nitrogen and carbon isotopes. Geochim. Cosmochim. Acta 65 (11), 1795–1808. https://doi.org/10.1016/S0016-7037(01)00554-3.

Garibotti, I.A., Vernet, M., Ferrario, M.E., et al., 2003. Phytoplankton spatial distribution patterns along the western Antarctic Peninsula (Southern Ocean). Mar. Ecol. Prog. Ser. 261, 21–39. https://doi.org/10.3354/meps261021.

Garrity, C., Ramseier, R.O., Peinert, R., et al., 2005. Water column particulate organic carbon modeled fluxes in the ice-frequented Southern Ocean. J. Mar. Syst. 56, 133–149. https://doi.org/10.1016/j.jmarsys.2004.09.009.

Geddes, J., Moore, G., 2007. A climatology of sea ice embayments in the Cosmonaut Sea. Antarctica. Geophysical Research Letters 34 (2), L02505. https://doi.org/10.1029/2006GL027910.

Gibson, J.A.E., Trull, T., Nichols, P.D., et al., 1999. Sedimentation of ^{13}C-rich organic matter from Antarctic sea-ice algae: A potential indicator of past sea-ice extent. Geology 27 (4), 331–334. https://doi.org/10.1130/0091-7613(1999)027.

Gloersen, P., Campbell, W.J., Cavalieri, D.J., et al., 1992. Arctic and Antarctic sea ice, 1978–1987: satellite passive-microwave observations and analysis. Research and Technology 77. https://doi.org/10.1016/0021-9169(95)90010-1.

Grose, M., McMinn, A., 2003. Algal biomass in east Antarctic pack ice: How much is in the east? Antarctic Biology in a Global Context 21–25.

Henley, S.F., Annett, A.L., Ganeshram, R.S., et al., 2012. Factors influencing the stable carbon isotopic composition of suspended and sinking organic matter in the coastal Antarctic sea ice environment. Biogeosciences 9 (3), 1137–1157. https://doi.org/10.5194/bg-9-1137-2012.

Heywood, K.R., Sparrow, M.D., Brown, J., et al., 1999. Frontal structure and antarctic bottom water flow through the Princess Elizabeth Trough. Antarctica. Deep-Sea Research I 46 (7), 1181–1200. https://doi.org/10.1016/S0967-0637(98)00108-3.

Holm-Hansen, O., Lorenzen, C.J., Holmes, R.W., et al., 1965. Fluorometric determination of chlorophyll. ICES J. Mar. Sci. 30, 3–15. https://doi.org/10.1093/icesjms/30.1.3.

Jia, R.M., Mu, X.Y., Chen, M., Zhu, J., Wang, B., Li, X.P., Astakhov, A.S., Zheng, M.F., Qiu, Y.S., 2020. Sources of particulate organic matter in the Chukchi and Siberian shelves: Clues from carbon and nitrogen isotopes. Acta Oceanol. Sin. 39 (9), 96–108.

Jia, R.M., Chen, M., Pan, H., et al., 2022. Freshwater components track the export of dense shelf water from Prydz Bay. Antarctica. Deep-Sea Research II 196, 42–53. https://doi.org/10.1016/j.dsr2.2022.105023.

Kennedy, H., Robertson, J., 1995. Variations in the isotopic composition of particulate organic carbon in surface waters along an 88 °W transect from 67 °S to 54 °S. Deep-Sea Res. II 42 (4–5), 1109–1122. https://doi.org/10.1016/0967-0645(95)00069-3.

Kennedy, H., Thomas, D.N., Kattner, G., et al., 2002. Particulate organic matter in Antarctic summer sea ice: concentration and stable isotopic composition. Mar. Ecol. Prog. Ser. 238, 1–13. https://doi.org/10.3354/meps238001.

Kopczynska, E.E., Goeyens, L., Semeneh, M., et al., 1995. Phytoplankton composition and cell carbon distribution in Prydz Bay, Antarctica: relation to organic particulate mater and its $\delta^{13}C$ values. J. Plankton Res. 17 (4), 685–707. https://doi.org/10.1093/plankt/17.4.685.

Lannuzel, D., Schoemann, V., Jong, J.D., et al., 2008. Iron study during a time series in the western Weddell pack ice. Mar. Chem. 108, 85–95. https://doi.org/10.1016/j.marchem.2007.10.006.

Lara, R.J., Alder, V., Franzosi, C.A., et al., 2010. Characteristics of suspended particulate organic matter in the southwestern Atlantic: Influence of temperature, nutrient and phytoplankton features on the stable isotope signature. J. Mar. Syst. 79 (1–2), 199–209. https://doi.org/10.1016/j.jmarsys.2009.09.002.

Liu, C.L., Niu, Y.Y., He, P.Q., 2021. Adaptation of polar ice algae to extreme sea-ice habitats: under the climate change conditions. Advances in Marine Science (in Chinese) 39 (2), 167–177. https://doi.org/10.3969/j.issn.1671-6647.2021.02.001.

Mariotti, A., Germon, J.C., Hubert, P., et al., 1981. Experimental determination of nitrogen kinetic isotope fractionation: Some principles, illustration for the denitrification and nitrification processes. Plant and Soil 62 (3), 413–430. https://doi.org/10.1007/BF02374138.

Martiny, A.C., Vrugt, J.A., Primeau, F.W., et al., 2013. Regional variation in the particulate organic carbon to nitrogen ratio in the surface waters. Global Biogeochem. Cycles 27 (3), 723–731. https://doi.org/10.1002/gbc.20061.

McMinn, A., Ryan, K.G., Ralph, P.J., et al., 2007. Spring sea ice photosynthesis, primary productivity and biomass distribution in eastern Antarctica, 2002–2004. Mar. Biol. 151 (3), 985–995. https://doi.org/10.1007/s00227-006-0533-8.

Meijers, A.J.S., Klocker, A., Bindoff, N.L., et al., 2010. The circulation and water masses of the Antarctic shelf and continental slope between 30 and 80 °E. Deep-Sea Res. II 57 (9–10), 723–737. https://doi.org/10.1016/j.dsr2.2009.04.019.

Misic, C., Harriague, A.C., Mangoni, O., et al., 2017. Effects of physical constraints on the lability of POM during summer in the Ross Sea. J. Mar. Syst. 166, 132–143. https://doi.org/10.1016/j.jmarsys.2016.06.012.

Moline, M.A., Prézelin, B.B., 1996. Long-term monitoring and analyses of physical factors regulating variability in coastal Antarctic phytoplankton biomass, in situ productivity, and taxonomic composition over subseasonal, seasonal and interannual time scales. Mar. Ecol. Prog. Ser. 145, 143–160. https://doi.org/10.3354/meps145143.

Moore, J.K., Abbott, M.R., 2000. Phytoplankton chlorophyll distributions and primary production in the Southern Ocean. J. Geophys. Res. Oceans 105, 28709–28722. https://doi.org/10.1029/1999JC000043.

Nelson, D.M., Smith, W.O., 1991. Sverdrup revisited: Critical depths, maximum chlorophyll levels, and the control of Southern Ocean productivity by the irradiance-mixing regime. Limnol. Oceanogr. 36 (8), 1650–1661. https://doi.org/10.4319/lo.1991.36.8.1650.

Nicol, S., Raymond, B., Meiners, K., 2010. BROKE-west, a large ecosystem survey of the south west indian ocean sector of the southern ocean (CCAMLR Division 58.4.2). Deep-Sea Res. II 57 (9–10), 693–700. https://doi.org/10.1016/j.dsr2.2009.11.002.

Ohshima, K.I., Fukamachi, Y., Williams, G.D., Nihashi, S., et al., 2013. Antarctic bottom water production by intense sea-ice formation in the cape darnley polynya. Nat. Geosci. 6 (3), 235–240. https://doi.org/10.1038/ngeo1738.

Orsi, A.H., Whitworth, T., Nowlin, W.D., 1995. On the meridional extent and fronts of the antarctic circumpolar current. Deep-Sea Research I 42 (5), 641–673. https://doi.org/10.1016/0967-0637(95)00021-w.

Orsi, A.H., Johnson, G.C., Bullister, J.L., 1999. Circulation, mixing, and production of antarctic bottom water. Prog. Oceanogr. 43 (1), 55–109. https://doi.org/10.1016/s0079-6611(99)00004-x.

Pakhomov, E.A., 2000. Demography and life cycle of Antarctic Krill, *Euphausia superba*, in the Indian sector of the Southern Ocean: Long-term comparison between coastal and open-ocean regions. Can. J. Fish. Aquat. Sci. 57, 68–90. https://doi.org/10.1139/cjfas-57-S3-68.

Pasquer, B., Mongin, M., Johnston, N., et al., 2010. Distribution of particulate organic matter (POM) in the Southern Ocean during BROKE-West (30 °E - 80 °E). Deep-Sea Research II 57 (9–10), 779–793. https://doi.org/10.1016/j.dsr2.2008.12.040.

Pollard, R.T., Lucas, M.I., Read, J.F., 2002. Physical controls on biogeochemical zonation in the Southern Ocean. Deep-Sea Research Part II 49 (16), 3289–3305. https://doi.org/10.1016/S0967-0645(02)00084-X.

Popp, B.N., Trull, T., Kenig, F., et al., 1999. Controls on the carbon isotopic composition of Southern Ocean phytoplankton. Global Biogeochem. Cycles 13 (4), 827–843. https://doi.org/10.1029/1999GB900041.

Pu, S.Z., Hu, X.M., Dong, Z.Q., et al., 2002. Features of circumpolar deep water, antarctic bottom water and their movement near the Prydz Bay. Acta Oceanologica Sinica (in Chinese) 24 (3), 1–8. https://doi.org/10.3321/j.issn:0253-4193.2002.03.001.

Rau, G.H., Takahashi, T., Des Marais, D.J., 1989. Latitudinal variations in plankton $\delta^{13}C$: implications for CO_2 and productivity in past oceans. Nature 341 (6242), 516–518. https://doi.org/10.1038/341516a0.

Raymond, B., Meiners, K., Fowler, C.W., et al., 2009. Cumulative solar irradiance and potential large-scale sea ice algae distribution off East Antarctica (30 °E – 150 °E). Polar Biol. 32 (3), 443–452. https://doi.org/10.1007/s00300-008-0538-5.

Redfield, A.C., Ketchum, B.H., Richards, F.A., 1963. The influence of organisms on the composition of seawater. The Sea 2, 26–77.

Ren, C.Y., Chen, M., Gao, Z.Y., et al., 2015. Stable carbon isotopic composition of suspended particulate organic matter in the Prydz Bay and its adjacent areas. Acta Oceanologica Sinica (in Chinese) 37 (12), 74–84. https://doi.org/10.3969/j.issn.0253-4193.2015.12.008.

Sarmiento, J.L., LeQuéré, C., 1996. Oceanic carbon dioxide uptake in a model of century-scale global warming. Science 274 (5291), 1346–1350. https://doi.org/10.1126/science.274.5291.1346.

Schmittner, A., Gruber, N., Mix, A.C., et al., 2013. Biology and air-sea gas exchange controls on the distribution of carbon isotope ratios ($\delta^{13}C$) in the ocean. Biogeosciences 10, 5793–5816. https://doi.org/10.5194/bg-10-5793-2013.

Smith, W.O., Asper, V.A., 2001. The influence of phytoplankton assemblage composition on biogeochemical characteristics and cycles in the Southern Ross Sea. Antarctica. Deep-Sea Research I 48, 137–161. https://doi.org/10.1016/S0967-0637(00)00045-5.

Smith, W.O., Lancelot, C., 2004. Bottom-up versus top-down control in phytoplankton of the Southern Ocean. Antarct. Sci. 16 (4), 531–539. https://doi.org/10.1017/S0954102004002305.

Smith, W.O., Nelson, D.M., 1985. Phytoplankton bloom produced by a receding ice edge in the Ross Sea: Spatial coherence with the density field. Science 227 (4683), 163–166. https://doi.org/10.1126/science.227.4683.163.

Smith, N.R., Dong,, Z.Q., Kerry, K.R., et al., 1984. Water masses and circulation in the region of Prydz Bay. Antarctica. Deep-Sea Research Part A 31 (9), 1121–1147. https://doi.org/10.1016/0198-0149(84)90016-5.

Soares, M.A., Bhaskar, P.V., Anilkumar, N., et al., 2020. Characteristics of particulate organic matter within the photic water column: A case study across the fronts in the Indian Sector of the Southern Ocean. Deep-Sea Research II 178. https://doi.org/10.1016/j.dsr2.2020.104851.

Stirnmann, L., Bornamn, T.G., Forrer, H.J., et al., 2024. A circum-Antarctic plankton isoscape: carbon export potential across the summertime Southern Ocean. Global Biogeochem. Cycles 38.

Talley, L.D., Pickard, G.L., Emery, W.J., et al., 2011. Descriptive physical oceanography: an introduction. Academic press, pp. 1–543. https://doi.org/10.1016/0011-7471(76)90868-8.

Talley, L.D., Feely, R.A., Sloyan, B.M., et al., 2016. Changes in ocean heat, carbon content, and ventilation: A review of the first decade of GO-SHIP global repeat

hydrography. Ann. Rev. Mar. Sci. 8, 185–215. https://doi.org/10.1146/annurev-marine-052915-100829.

Tao, S.Q., Li, Y.H., Tang, Z., et al., 2022. Composition of organic materials and the control factors of suspended particulates in the surface water of the Ross Sea-Amundsen Sea in marginal sea of the southwestern Antarctic in austral summer 2019–2020. Marine Geology & Quaternary Geology (in Chinese) 42 (4), 24–38. https://doi.org/10.16562/j.cnki.0256-1492.2022022101.

Tripathy, S.C., Pavithran, S., Sabu, P., et al., 2015. Deep chlorophyll maximum and primary productivity in Indian Ocean sector of the Southern Ocean: Case study in the Subtropical and Polar Front during austral summer 2011. Deep-Sea Res. II 118, 240–249. https://doi.org/10.1016/j.dsr2.2015.01.004.

Trull, T.W., Armand, L., 2001. Insights into Southern Ocean carbon export from the $\delta^{13}C$ of particles and dissolved inorganic carbon during the SOIREE iron release experiment. Deep-Sea Res. II 48 (11–12), 2655–2680. https://doi.org/10.1016/S0967-0645(01)00013-3.

Trull, T.W., Davies, D., Casciotti, K., 2008. Insights into nutrient assimilation and export in naturally iron-fertilized waters of the Southern Ocean from nitrogen, carbon and oxygen isotopes. Deep-Sea Res. II 55 (5–7), 820–840. https://doi.org/10.1016/j.dsr2.2007.12.035.

Van Leeuwe, M.A., Tedesco, L., Arrigo, K.R., et al., 2018. Microalgal community structure and primary production in Arctic and Antarctic sea ice: A synthesis. Elementa-Science of the Anthropocene 6. https://doi.org/10.1525/elementa.267.

Venturini, N., Zhu, Z., Bessonart, M., et al., 2020. Between-summer comparison of particulate organic matter in surface waters of a coastal area influenced by glacier meltwater runoff and retreat. Polar Sci. 26, 10.1016/j.polar.2020.100603.

Wakatsuchi, M., Ohshima, K., Hishida, M., et al., 1994. Observations of a street of cyclonic eddies in the indian-ocean sector of the antarctic divergence. J. Geophys. Res. 99, 20417–20426. https://doi.org/10.1029/94jc01478.

Westwood, K.J., Brian, G.F., Meiners, K.M., et al., 2010. Primary productivity off the Antarctic coast from 30°–80 °E; BROKE-West survey, 2006. Deep-Sea Res. II 57 (9–10), 794–814. https://doi.org/10.1016/j.dsr2.2008.08.020.

Whitworth III T, Orsi A H, Kim S-J, et al. 1985. Water masses and mixing near the Antarctic Slope Front. In: Jacobs S S, Weiss R F, eds. Ocean, Ice, and Atmosphere: Interactions at the Antarctic Continental Margin, AGU, Antarctic Research Series, Volume 75 https://doi.org/10.1029/AR075p0001.

Wilkes, E.B., Pearson, A., 2019. A general model for carbon isotopes in red-lineage phytoplankton: interplay between unidirectional processes and fractionation by RubisCO. Geochim. Cosmochim. Acta 265, 163–181. https://doi.org/10.1016/j.gca.2019.08.043.

Williams, G.D., Nicol, S., Aoki, S., et al., 2010. Surface oceanography of BROKE-West, along the Antarctic margin of the south-west Indian Ocean (30–80 °E). Deep-Sea Res. II 57 (9–10), 738–757. https://doi.org/10.1016/j.dsr2.2009.04.020.

Wong, W.W., Sackett, W.M., 1978. Fractionation of stable carbon isotopes by marine phytoplankton. Geochim. Cosmochim. Acta 42, 1809–1815. https://doi.org/10.1016/0016-7037(78)90236-3.

Wright, S.W., van den Enden, R.L., Pearce, I., et al., 2010. Phytoplankton community structure and stocks in the Southern Ocean (30–80 °E) determined by CHEMTAX analysis of HPLC pigment signatures. Deep-Sea Res. II 57 (9–10), 758–778. https://doi.org/10.1016/j.dsr2.2009.06.015.

Zhang, R., Zheng, M.F., Chen, M., et al., 2014. An isotopic perspective on the correlation of surface ocean carbon dynamics and sea ice melting in Prydz Bay (Antarctica) during austral summer. Deep-Sea Research I 83, 24–33. https://doi.org/10.1016/j.dsr.2013.08.006.